Geochimica et Cosmochimica Acta Vol. 45, pp. 1281 to 1289, 1981
Printed in Great Britain

0016-7037/81/081281-09$02.00/0
Pergamon Press Ltd

Crystal growth of calcite from calcium bicarbonate solutions at constant P_{CO_2} and 25°C: a test of a calcite dissolution model

MICHAEL M. REDDY*
Division of Laboratories and Research, New York State Department of Health, Albany, NY 12201, U.S.A.

L. NIEL PLUMMER and E. BUSENBERG
U.S. Geological Survey, Reston, VA 22092, U.S.A.

(*Received* 9 *September* 1980; *accepted in revised form* 17 *March* 1981)

Abstract—A highly reproducible seeded growth technique was used to study calcite crystallization from calcium bicarbonate solutions at 25°C and fixed carbon dioxide partial pressures between 0.03 and 0.3 atm. The results are not consistent with empirical crystallization models that have successfully described calcite growth at low P_{CO_2} ($<10^{-3}$ atm). Good agreement was found between observed crystallization rates and those calculated from the calcite dissolution rate law and mechanism proposed by PLUMMER *et al.* (1978).

INTRODUCTION

HETEROGENEOUS reactions involving calcium carbonate are of considerable importance in hydrochemical environments. Recent concern about global carbon dioxide accumulation (BROECKER *et al.*, 1979) and the influence of acid precipitation on stream water chemistry has emphasized the significance of carbonate mineral reactions (JOHNSON, 1979). To formulate models of these reactions, accurate rates, rate laws and reaction mechanisms must be available. However, as several authors have observed, the kinetics of heterogeneous reactions in geochemical systems are not well defined (BERNER, 1978; NANCOLLAS *et al.*, 1979; PLUMMER *et al.*, 1979).

Use of kinetic data on carbonate mineral reactions to model environmental processes requires definition of many factors, including saturation state, P_{CO_2}, pH, reacting surface area, solution ionic composition, inhibiting substances and hydrodynamics.

Recent studies of the crystal growth and dissolution kinetics of calcite have helped to define the reaction mechanism. Nancollas and Reddy, using a highly reproducible seeded growth technique, examined calcite crystallization near pH 9 and developed both a reaction rate law and a crystallization mechanism (NANCOLLAS and REDDY, 1971, 1974a, b; REDDY and NANCOLLAS, 1971, 1973, 1976; REDDY, 1975, 1977, 1978, 1979). PLUMMER *et al.* (1978) presented a mechanistic model for calcite dissolution that applies over a wide range of solution pH and P_{CO_2}. The rate expression proposed by Plummer and co-workers contains an explicit term describing backward reaction for dissolution (i.e. crystallization).

A test of the backward rate dependence of the dissolution model was attempted by PLUMMER *et al.* (1979) using REDDY's (1975) low-P_{CO_2} crystal-growth data ($P_{CO_2} = 10^{-3.5}$ to $10^{-3.3}$ at pH = 8.6–8.9). They concluded that if this backward rate dependence is correct, the surface P_{CO_2} under Reddy's experimental conditions must be initially somewhat greater than that of bulk fluid, and as the reaction approaches equilibrium with calcite, surface P_{CO_2} must change to that of the bulk fluid. However, experimental data to verify this influence have not been available.

Surface layer P_{CO_2} is critical in the dissolution model because it is used to define the equilibrium composition of the adsorption layer. The dissolution model of PLUMMER *et al.* (1979) assumes an adsorption layer, consisting of fully or partially hydrated ions or molecules adsorbed to the crystal surface. Thickness of the layer probably ranges from 10 to 100 Å. Solute from the supersaturated solution reaches this adsorption layer by mass transfer through a hydrodynamic boundary layer, an assumed thin stagnant volume of solution adjacent to the crystal surface. In the case of a laminar hydrodynamic boundary layer mass transfer through this region occurs via molecular diffusion. Depending upon experimental conditions, the hydrodynamic boundary layer can vary in thickness from 20 to 150 μm. A discussion of the adsorption layer, and the hydrodynamic boundary layer is given by MULLIN (1972). It was suggested (PLUMMER *et al.*, 1978) that at relatively *high* P_{CO_2} (>0.03 atm) the flux of CO_2 between the reacting crystal surface and the bulk fluid is large relative to the total CO_2 concentration, so that surface P_{CO_2} is very near the bulk fluid value. Results of calcite dissolution experiments at high P_{CO_2} (PLUMMER *et al.*, 1978) support this conclusion. At low

* Present address: U.S. Geological Survey, Box 25046, Mail Stop 407, Federal Center, Denver, CO 80225, U.S.A.

bulk fluid P_{CO_2}, however, the surface P_{CO_2} may depend significantly on the CO_2-flux between the surface and the bulk fluid (PLUMMER *et al.*, 1979).

To test the backward rate dependence of the dissolution model, crystal growth of calcite must therefore be studied at high bulk fluid P_{CO_2}. Because no such growth experiments have been published, we have measured calcite crystallization rates at high P_{CO_2} (by the seeded growth technique used previously) and have compared the results with predictions based on the dissolution model.

EXPERIMENTAL

Materials

Analytical reagent-grade chemicals, doubly distilled water and grade A glassware were used throughout. Two calcite powders were used as seed material. Seed crystal A (Baker* $CaCO_3$ No. 1294, Lot 38767) has a specific surface area of 0.228 m^2/g as measured by a single point BET method using a 30% N_2–70% He gas mixture with a Quantachrome Corp. Monosorb surface area analyzer. Seed crystal B (Fisher $CaCO_3$ No. C-65, Lot 775084) has a specific area of 0.699 m^2/g and was measured by Micromeritics Inc., using a multipoint Kr gas BET procedure. Scanning electron microscopy showed both seed materials to consist of uniform rhombs with a narrow size distribution.

Crystallization experiments were conducted in a 1-l. water-thermostated (25.0 ± 0.1°C) double-walled vessel. To minimize mixing of room air with gas mixtures the vessel was covered with a close-fitting Plexiglas top with removable entry port. The solutions were stirred with a three-bladed polyethylene propeller at a constant rate of 350 rpm. Water-saturated gas mixtures (30, 10 and 3% carbon dioxide in nitrogen) were bubbled into the crystallizing solution at a rate of several liters per minute to maintain a constant P_{CO_2}. The gas mixtures (Air Products) were prepared by weight and were found accurate to within 1% of their stated composition by gas chromatography.

An Orion Research Ionalyzer (model 801) and a digital printer (model 751) were used to measure and continually record pH. The Sargent Welch combination electrodes were filled with saturated KCl and were calibrated with Fisher Scientific Company pH 4.01 ± 0.01 and 6.86 ± 0.01 buffers before and after each experiment.

Preparation of supersaturated solutions

Stable supersaturated calcium bicarbonate solutions were prepared from stock solutions saturated with respect to calcite and carbon dioxide at 4°C. This technique utilizes the fact that calcite solubility increases with decreasing temperature. The stock solutions were prepared by adding 50 g of seed B to 2 l. of freshly distilled water stirred at 4°C with 100% CO_2 bubbled for a period of 24 hr. The solutions were then rapidly filtered through 0.45 μm Millipore filters and stored in a refrigerator near 4°C until needed.

Shortly before each experiment 500 ml of the stock solution were filtered through a 0.22 μm Millipore filter into a volumetric flask. This solution was quantitatively transferred to the reaction vessel. After reaching constant temperature and P_{CO_2}, the pH was monitored for consistancy to verify metastability. Constant solution pH demonstrated supersaturated solution metastability since crystallization was accompanied by a drop in solution pH. A sample of the supersaturated solution was analyzed for Ca before the start of each experiment to confirm the solution's metastability.

The outlined procedure was used to prepare the supersaturated solution because: (1) the same $CaCO_3$ material could be used both as seed and to prepare the supersaturated solutions; (2) the solution could be stored for extensive periods of time; and (3) several initial supersaturated solutions could be prepared by raising the solutions temperature to 25°C and varying the P_{CO_2}.

Analysis of the solutions

The solution in the reaction vessel was sampled with a plastic syringe and filtered through 0.22 μm Millipore filters. The Ca concentrations were determined in duplicate by EDTA titration with a 2.5 ml microburette using the fluorescence endpoint of calcein and the procedure described by DIEHL (1964). The reproducibility of the Ca analysis was better than 0.5%.

Seeded-growth experiments

In a typical seeded-growth experiment 500 mg of calcite seed was inoculated into 500 ml of stirred supersaturated solution (Table 1). During the reaction, samples were removed, filtered, and analyzed for total Ca as described above.

* The use of brand names in this report is for identification purposes only and does not imply endorsement by the United States Geological Survey, or by the New York State Department of Health.

Table 1. Initial conditions and calculated equilibrium point for calcite growth from calcium bicarbonate solutions at fixed P_{CO_2} and 25°C

Run number	Seed material	Seed concentration (g/l)	P_{CO_2} (atm)	Initial calcium (mmol/l)	Calculated [1] initial values		Calculated [1] equilibrium values	
					pH	Ω	$pH_{(s)}$	Total calcium (mmol/l)
3	A	1.07	0.289	12.55	6.686	7.32	6.348	5.740
4	A	1.03	0.289	12.94	6.711	7.90	6.348	5.740
5	B	1.02	0.289	12.97_5	6.694	7.95	6.348	5.740
6	A	1.03	0.0959	12.66_3	7.143	22.19	6.658	3.781
7	A	1.06	0.0287	12.73_2	7.641	71.10	6.998	2.420
8	B	0.98	0.0288	11.78_5	7.604	58.98	6.997	2.422
9	B	1.00	0.0958	12.13_2	7.142	19.99	6.658	3.779

[1] Thermodynamic calculations use the aqueous model described in the text and data of Table 2.

Table 2. Thermodynamic data at 25°C for the system $CaCO_3 - CO_2 - H_2O$

Reaction	log K	Source
$CaCO_3$ (Calcite) = $Ca^{2+} + CO_3^{2-}$	- 8.475	Jacobson and Langmuir (1974)
$CO_2 + H_2O = H_2CO_3^*$	- 1.466	Harned and Davis (1943)
$H_2CO_3^* = H^+ + HCO_3^-$	- 6.351	Harned and Davis (1943)
$HCO_3^- = H^+ + CO_3^{2-}$	-10.330	Harned and Scholes (1941)
$CaHCO_3^+ = Ca^{2+} + HCO_3^-$	- 1.015	Jacobson and Langmuir (1974)
$CaCO_3^0 = Ca^{2+} + CO_3^{2-}$	- 3.153	Reardon and Langmuir (1974)
$H_2O = H^+ + OH^-$	-14.000	Helgeson (1969)

Calculation of saturation state of solutions

The progress of the reaction was followed in terms of the saturation state of the solution, Ω, defined as the ratio of the calcite ion activity product (IAP) in solution to the calcite equilibrium constant (K_{sp}) for the reaction $CaCO_3 = Ca^{2+} + CO_3^{2-}$. The IAP was calculated from the measured Ca and P_{CO_2} using the aqueous model of Table 2, which assumes the presence of Ca^{2+}, $CaHCO_3^+$, $CaCO_3^0$, $H_2CO_3^*$ (where $H_2CO_3^* = H_2CO_3^0 + CO_{2aq}$ by convention), HCO_3^-, CO_3^{2-}, H^+ and OH^-. Single ion activity coefficients of charged species were calculated from the extended Debye–Hückel expressions as used in WATEQ (TRUESDELL and JONES, 1974) and WATEQF (PLUMMER *et al.*, 1976). Similar thermodynamic calculations using the measured pH (with total Ca or P_{CO_2}) rather than the preferred total Ca and P_{CO_2} to define IAP were judged less reliable owing to uncertainties in the measurement of pH in the stirred calcite suspensions.

RESULTS

Calcite crystallization rates

Several parameters essential in depicting the calcite crystallization process, including solution supersaturation and temperature, have been quantitatively related to crystallization rates in previous studies near pH 9 and 10^{-3} atm P_{CO_2} (NANCOLLAS and REDDY, 1971). The stirring rate was shown to have no effect on the crystallization rate, supporting the concept of an interfacial rate-determining step*. The influence of higher solution P_{CO_2} (and lower pH) had not been investigated.

Initial solution conditions for our growth experiments are shown in Table 1, along with the type and amount of seed used and the calculated equilibrium points. Calcite growth began immediately upon inoculation, as indicated by a sharp drop in solution pH. The total calcium concentration decreased smoothly with time with each seed material and at each P_{CO_2} (Fig. 1). Seed B, with a higher surface area, approached equilibrium more rapidly.

Calcite crystallization rates were calculated as instantaneous slopes at each sampling time from the plots of total calcium concentration versus time (Fig. 1). The calculated rates were then normalized to unit surface area ($mmol \cdot cm^{-2} \cdot sec^{-1}$) so that growth rates for the two seeds could be compared.

Calcite growth rates as a function of solution total calcium concentration for each P_{CO_2} (Fig. 2) are curved at high solution supersaturations, corresponding to experiments at lower P_{CO_2}. At lower supersaturation values (30% CO_2) the reaction rate approached a linear function of solution total calcium concentration. The lack of evidence for either a growth surge at the onset of the experiment (Fig. 1) or a discontinuous drop in reaction rate at low supersaturation (Fig. 2) indicates the absence of secondary nucleation and growth inhibition.

The close agreement of the normalized rates for seeds A and B (Fig. 2) indicates that the observed differences between experimental rates (Fig. 1) are due solely to the differences in their areas for growth. Differences in their growth-site density (i.e. dislocation site density) do not appear significant.

Runs 7, 9, and 3 (in 3, 10, and 30% CO_2, respectively) were reacted for longer times and are within 0.0, 0.2, and 0.4 mmoles per liter total Ca, respectively, of the theoretical equilibrium value (Table 2) after approximately 18 hr of reaction (Fig. 1). Since the solubilities of unstable calcium carbonate polymorphs lie above these values, this is evidence for the expected formation of calcite, rather than of less stable calcium carbonate polymorphs. Calcite growth in the pure calcium bicarbonate solutions used here does not

* The crystallization process can be divided into two steps: (1) a diffusional process, involving solute mass transport across the hydrodynamic boundary layer; and (2) a crystal surface incorporation reaction whereby solute molecules dehydrate and arrange themselves into the crystal lattice. If the diffusional resistance is low (that is the rate of mass transport across the hydrodynamic boundary layer is much greater than the rate of solute incorporation at the crystal surface) then the crystallization rate will be governed by the rate of surface integration. This overall rate determining surface integration process is often termed the 'interfacial rate determining step'.

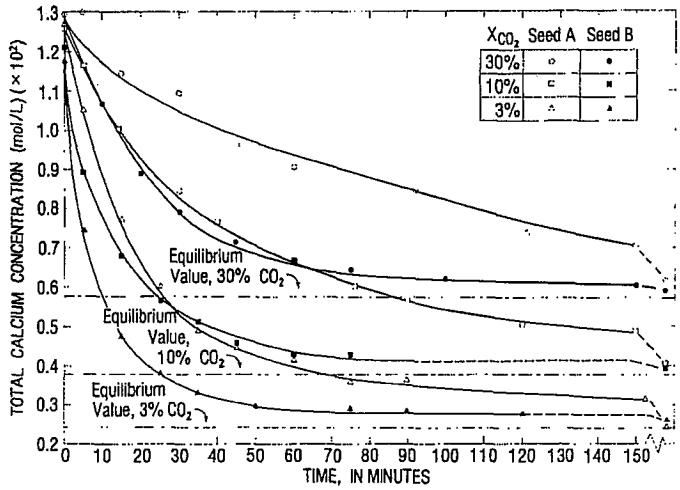

Fig. 1. Total calcium as a function of time for crystal growth at three CO_2 partial pressures and 25°C. Horizontal lines indicate calculated equilibrium concentrations for each gas composition (X_{CO_2} in % CO_2). Final points are at times between 300 and 1000 min.

cease below a critical calcium concentration, unlike crystallization in more soluble salt systems (MULLIN and OSMAN, 1973).

The dependence of reaction rate on P_{CO_2} is shown in Fig. 3, in which crystallization rates are plotted as a function of solution supersaturation, Ω. The rate of calcite growth at a fixed crystallization driving force varied in a complex manner with increasing P_{CO_2} and Ω. At low Ω crystallization rates increase with increasing P_{CO_2} while at high Ω the opposite is true.

The nonlinearity of the relationship between log rate and log Ω (Fig. 3) demonstrates the lack of suitability of an empirical rate expression similar to the equation

$$R = k\Omega^n \quad (1)$$

(where k and n are constants) for describing calcite crystal growth at constant P_{CO_2} between 0.03 and 0.3 atm and 25°C. A least squares best fit statistical analysis of all rate data with eqn (1) showed that both constants (k and n) varied with solution P_{CO_2} and Ω in an unpredictable fashion. The variation in reaction order (n) was felt to be strong evidence against the use of eqn (1) for data analysis. Plots of log rate are also nonlinear functions of log ($\Omega - 1$) and log ($C - Cs$), where C is total Ca and Cs is total Ca at equilibrium for the run. Thus, none of the commonly recognized empirical expressions are appropriate for describing calcite growth under the experimental conditions.

Comparison of experimental rates with the dissolution model

PLUMMER *et al.* (1978) studied the dissolution of calcite in CO_2–H_2O solutions, using pH-stat and free

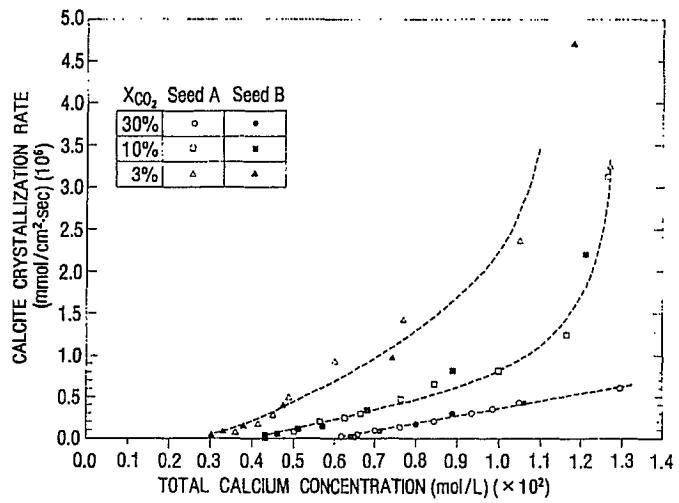

Fig. 2. Rate of calcite growth, normalized to unit surface area, as a function of solution total calcium concentration at constant P_{CO_2} and 25°C. (X_{CO_2} is % CO_2 in the gas mixture).

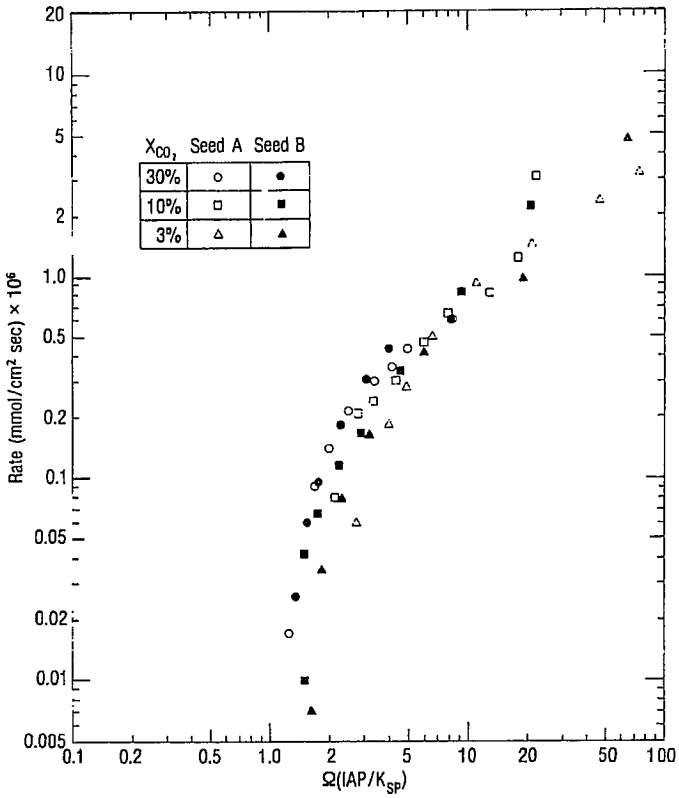

Fig. 3. Log–log plot of calcite growth rate as a function of supersaturation, Ω. Data between Ω of 2 and 10 indicate that growth rate at constant Ω depends on P_{CO_2}. The nonlinearity demonstrates growth rate is not described by an empirical exponential relationship of Ω.

drift methods, over pH ranges from about 2–7, P_{CO_2} from 0.0003 to 0.97 atm, and temperature from 5 to 60°C. They proposed that three reactions:

$$CaCO_3 + H^+ = Ca^{2+} + HCO_3^- \quad (2)$$

$$CaCO_3 + H_2CO_3^0 = Ca^{2+} + 2HCO_3^- \quad (3)$$

$$CaCO_3 + H_2O = Ca^{2+} + HCO_3^- + OH^- \quad (4)$$

occur simultaneously on the calcite surface and that the net rate of dissolution, R, is given by

$$R = k_1 a_{H^+} + k_2 a_{H_2CO_3^*} + k_3 a_{H_2O} - k_4 a_{Ca^{2+}} a_{HCO_3^-} \quad (5)$$

where a_i denotes thermodynamic activity of the ith ion and k_1, k_2 and k_3 are the respective rate constants for reactions (2–4). The backward reaction rate constant, k_4, depends on temperature and P_{CO_2}. Theoretical calculations show that k_4 is

$$k_4 = \frac{K_2}{K_{sp}}\left[k_1' + \frac{1}{a_{H^+(s)}}(k_2 a_{H_2CO_3(s)} + k_3 a_{H_2O(s)})\right], \quad (6)$$

which agrees well with observed values of k_4 (PLUMMER *et al.*, 1978). In eqn (6) K_2 is the second dissociation constant of carbonic acid and K_{sp} is the calcite equilibrium constant (Table 2). The term k_1' is the first-order mechanistic rate constant for H^+ attack (2) and may be 10–20 times larger than the measured k_1, which was interpreted as the H^+ transport rate constant. The subscript (s) denotes values on the calcite surface. Equation (5) can be expressed in Ω notation as

$$R = \alpha + \beta - \left(\alpha + \frac{a_{H^+}}{a_{H^+(s)}}\beta\right)\Omega \quad (7)$$

where $\alpha \simeq k_1 a_{H^+}$ and $\beta = k_2 a_{H_2CO_3^*} + k_3 a_{H_2O}$ (PLUMMER *et al.*, 1979).

The reaction mechanism is interpreted as follows: Reaction of calcite with H^+ is very fast, while reaction with $H_2CO_3^*$ and H_2O is significantly slower. At relatively high P_{CO_2} (as in the experiments reported here) the surface P_{CO_2} is probably near the bulk fluid value. At P_{CO_2} <3% the surface P_{CO_2} tends to be less than the bulk fluid value during dissolution and greater than the bulk fluid value during crystallization (PLUMMER *et al.*, 1979). The surface activity of H_2O is always near the bulk fluid value. Because reaction with H^+ is fast, the a_{H^+} in the surface layer, $a_{H^+(s)}$, is the equilibrium value for calcite at the surface P_{CO_2} and activity of water. (See Table 1 for values of $pH_{(s)}$.)

Equations (5–7) show that calculation of rate requires use of an aqueous model to define the speciation and saturation state of the solution. To compare the calculated and observed rates, we have used the aqueous model (Table 2) to calculate solution specia-

tion and Ω at each measured calcium concentration and accompanying P_{CO_2} value. The following values for the terms in eqn (7) were used in the calculation of rate:

(1) a_{H^+} and Ω in the bulk fluid were calculated from the observed total calcium and bulk solution P_{CO_2} using the aqueous model (Table 2).

(2) $a_{H_2CO_3^*}$ was calculated from P_{CO_2} (Table 1) and Henry's law constant for CO_2 (Table 2).

(3) The activity of H_2O was taken as unity.

(4) k_1, k_2, and k_3 were, respectively, 0.051, 3.45×10^{-5}, and 1.19×10^{-7} cm/sec (PLUMMER *et al.*, 1978). Because H^+ contributes little to the forward rate, the calculated results are not sensitive to our uncertainty in the value of k_1'.

(5) $a_{H(s)}$ was calculated from the aqueous model and assumed calcite equilibrium at the surface P_{CO_2}. The surface P_{CO_2} in turn was assumed to be equal to the bulk fluid value.

Essentially all of the calculated rates are within a factor of three of the observed rates while the observed rates varied over more than three orders of magnitude and Ω varied over several decades (Fig. 4). Calculated rates for 30% CO_2 were two to three times faster than the observed rate near equilibrium. Calculated rates for low P_{CO_2} were generally closer to the observed values (Fig. 4). As equilibrium was approached, the calculated rate tended to be faster than the observed rate. Differences between calculated and observed crystallization rates may arise from a number of factors including: uncertainties in thermodynamic data and rate constants used in the rate calculation; the influence of growth inhibitors at trace concentrations; and changes in crystallization mechanism at low supersaturation. In addition, calcite crystallization and dissolution reactions examined in this study and that of PLUMMER *et al.* (1979) were characterized, for the most part, well away from equilibrium. Thus, the experimental data base would accentuate deviations of calculated rates from measured rates near equilibrium.

It should be emphasized that the results discussed here were obtained to test the predictability (and thus the rate expression and mechanism) of the calcite dissolution model of PLUMMER *et al.* (1978). Calcite crystallization rates varied by more than three orders of magnitude within a wide range of P_{CO_2} and Ω values. Over this range of conditions and observed rates the dissolution model predicted the absolute crystallization rates of two different seed materials to within a factor of 2 for many reaction points. Several data points exhibited significantly better agreement. This agreement is felt to be appropriate evidence in support of the dissolution model of PLUMMER *et al.* (1978) since calculated precipitation rates often are orders of magnitude in error (KOUTSOUKOS *et al.*, 1980) and since crystallization parameters cannot be typically determined with an accuracy better than about a factor 2 (GARSIDE, 1977).

A further test of the consistency of the dissolution model of PLUMMER *et al.* (1978) with the calcite growth data is provided by plotting the observed growth in the form of the dissolution rate eqn (5), i.e. plotting $R_{obs} - k_1 a_{H^+}$ vs $a_{Ca^{2+}} a_{HCO_3^-}$. From eqn (5), at constant P_{CO_2} and a_{H_2O} (as in our experiments) such plots should be linear with slope of $-k_4$ and a y-intercept (at $a_{Ca^{2+}} a_{HCO_3^-} = 0$) equal to $k_2 a_{H_2CO_3^*} + k_3 a_{H_2O}$. Figure 5 shows that these plots, for each P_{CO_2} studied, are linear and pass through the equilibrium point, as required by the model of PLUMMER *et al.* (1978). Close agreement was obtained in duplicate runs at 3 and 10% CO_2 and in triplicate runs at 30% CO_2.

The observed and calculated slopes (k_4) and intercepts ($k_2 a_{H_2CO_3^*} + k_3 a_{H_2O}$) from Fig. 5 (Table 3) agreed within a factor of two. At 3% CO_2 the observed slope for run 7 is slightly higher than the slope (k_4) calcu-

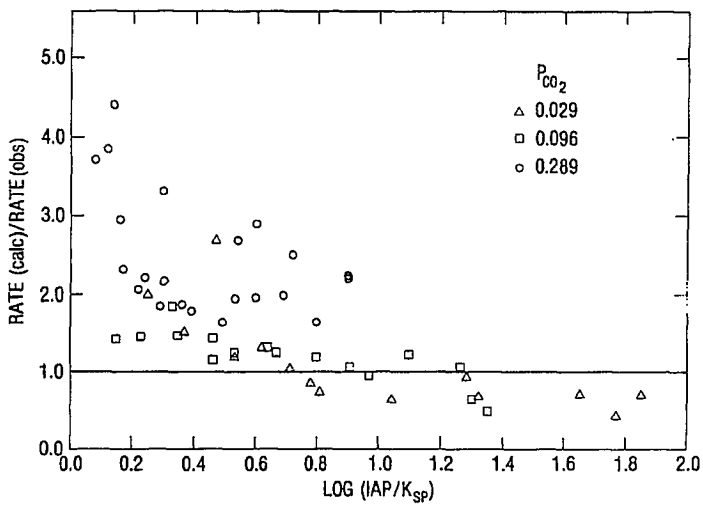

Fig. 4. Comparison of calculated and observed growth rates as a function of solution supersaturation.

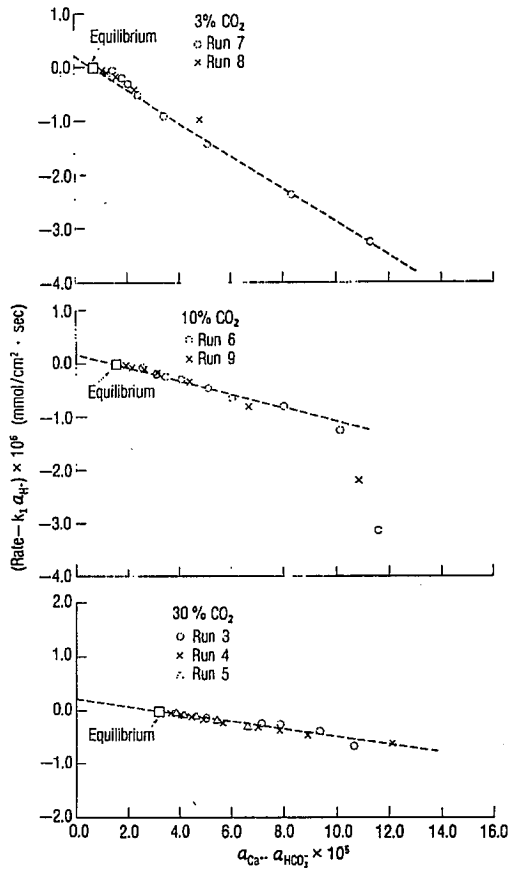

Fig. 5. Calcite growth data plotted in the form of the dissolution rate equation (eqn 5). The y-intercept (at $a_{Ca^{2+}} \cdot a_{HCO_3^-} = 0$) corresponds to the term $k_2 a_{H_2CO_3^*} + k_3 a_{H_2O}$, and the slope corresponds to k_4. Initial data points for growth at 10% CO_2 (center plot) appear to deviate significantly from the best fit line. This apparent deviation may be due to errors associated with reaction rate measurements at zero time.

lated from eqn (6), but near equilibrium, the data points for both runs lie closer to the calculated slope (Table 3). The y-intercept at this P_{CO_2} (at $a_{Ca^{2+}} \cdot a_{HCO_3^-} = 0$) is slightly higher than predicted. The observed slopes and intercepts for two runs at 10% CO_2 are nearly identical to those predicted by eqns (5) and (6) (Table 3). For 30% CO_2 the observed slope and intercept are twice the calculated values.

In calculating the slopes and intercepts it was assumed that k_1, k_2 and k_3 have values identical to those measured by PLUMMER *et al.* (1978) for the dissolution of Iceland spar, a semioptical calcite of natural origin. By assuming equivalence of rate constants for the two calcites, it is implied that the reaction site density per unit area for the seeds used and Iceland spar is similar. Because reaction sites include surface imperfections in the crystal structure, the more perfectly grown seed material has a smaller reaction site density per unit area, and thus k_1, k_2 and k_3 should be smaller values for more perfect seed crystals. (Iceland spar powder, prepared by grinding the natural mineral, would be expected to have a higher surface defect density than the calcite seed crystals A and B which were prepared by precipitation from aqueous solution.) If the rate constants were smaller than those for Iceland spar, the calculated intercepts (Table 3) would be smaller. For example, the discrepancy between calculated and observed intercepts at 30% CO_2 implies that the reaction-site density of the seed material is approximately half that of Iceland spar. Yet the observed intercept at 10% is nearly identical to the theoretical value and larger than the theoretical value at 3% CO_2. Thus uncertainties in reaction site density alone cannot account for all the differences between experiment and mechanistic model.

Release of CO_2 at the crystal surface during precipitation causes the surface P_{CO_2} to be larger than the bulk fluid value. This value for the surface P_{CO_2} depends (at least in part) on the calcite growth rate, the rate of hydrodynamic transport of CO_2 from the surface to the bulk fluid and thence into the bubbled gas phase. Although the true value of surface P_{CO_2} is difficult to estimate, it should be somewhat larger than the bulk fluid value during crystal growth. If the reaction-site density of the seed material is half that of Iceland spar, the observed intercepts for both runs at 3 and 10% CO_2 indicate that the surface P_{CO_2} is several times larger than the bulk fluid value. Because surface P_{CO_2} appears to be very near the bulk fluid value at similar (but opposite) Ca^{2+}–HCO_3^- flux conditions during calcite dissolution (PLUMMER *et al.*,

Table 3. Comparison of observed and calculated slopes and intercepts

		Observed[1/]		Calculated[2/]	
Runs	%CO_2	Slope	y-Intercept	Slope (k_4)	y-Intercept ($k_2 a_{H_2CO_3^*} + k_3 a_{H_2O}$)
7,8	3.	-3.1×10^{-2}	0.20×10^{-6}	-2.0×10^{-2}	0.15×10^{-6}
6,9	10.	-1.3×10^{-2}	0.20×10^{-6}	-1.6×10^{-2}	0.23×10^{-6}
3,4,5	30.	-0.7×10^{-2}	0.20×10^{-6}	-1.5×10^{-2}	0.46×10^{-6}

1/ From Fig. 5.

2/ Equations 5 and 6.

1978), it is unlikely that surface P_{CO_2} is actually several times the bulk fluid value in the present growth experiments. Furthermore, if surface P_{CO_2} varied by a factor of two during growth, eqn (6) indicates that the plots of Fig. 5 should be curves rather than the observed straight lines. The linear relationships of Fig. 5 indicate constant surface P_{CO_2} for the duration of the runs at 30 and 10% CO_2. At 3% CO_2, there is a suggestion that the initial surface P_{CO_2} is higher and decreases slightly as equilibrium is approached (Fig. 5).

Although there is considerable agreement between the growth data and the dissolution model of PLUMMER *et al.* (1978), uncertainties of a factor of two remain in the calculated and observed rates. The deviations are most pronounced at high P_{CO_2} and low supersaturations. They may be due to failure to include an additional reaction step in the overall reaction mechanism, or to reduction in growth site density or to a crystallization mechanism change as the reaction approaches equilibrium. Additional experimental investigation may lead to a fuller understanding of the discrepancies between the calculated and observed calcite crystallization rates.

CONCLUSIONS

Our results show agreement within a factor of two between measured crystallization rates of calcite and the rates predicted from the PLUMMER *et al.* (1978) mechanistic model for calcite dissolution. The observed rate data also follow the form of the rate equation found for calcite dissolution. The measured rates were determined with three separate seed materials—two used for our growth experiments and the Iceland spar crystals used to develop the dissolution rate model. These findings suggest that appropriately interpreted dissolution measurements could be used to predict crystallization reaction rates.

Crystallization is generally considered a multistep process, in which ion incorporation at a surface growth site is often rate-determining (NANCOLLAS and PURDIE, 1964). Dissolution, in contrast, is frequently diffusion-limited. For calcite, in the pH range examined here, a surface reaction is rate-limiting for both the growth and dissolution steps. Thus the agreement between the measured rates of crystallization and those predicted from the dissolution rate expression appears to result from similar forward and backward rate-limiting steps, i.e. ion incorporation or release at a dislocation site on the crystal surface.

Note added in proof

Recent reports, which appeared in print following submission of this manuscript for publication, examine the application of the PLUMMER *et al.* (1978) rate expression to experimental growth of calcite (HOUSE, 1981a, b) and the formation of caves by calcite dissolution (DREYBRODT, 1981).

REFERENCES

BERNER R. A. (1978) Rate control of mineral dissolution under earth surface conditions. *Am. J. Sci.* **278**, 1235–1252.

BROECKER W. S., TAKAHASHI T., SIMPSON H. J. and PENG T.-H. (1979) Fate of fossil fuel carbon dioxide and the global carbon budget. *Science* **206**, 409–418.

DIEHL H. (1964) *Calcein, Calmagite, and o,o'-dihydroxyazobenzene. Titrimetric, Colorimetric and Fluorometric Reagents for Calcium and Magnesium.* The G. Frederick Smith Chemical Co., Columbus, Ohio. 124 pp.

DREYBODT W. (1981) Kinetics of the dissolution of calcite and its applications to karstification. *Chem. Geol.* **31**, 245–269.

GARSIDE J. (1977) Kinetics of crystallization from solution. In *1976 Crystal Growth and Materials* (eds E. Kaldis and H. J. Scheel), pp. 483–513. North Holland.

HARNED H. S. and SCHOLES S. R. JR (1941) The ionization constant of HCO_3^- from 0 to 50 . *Am. Chem. Soc. J.* **63**, 1706–1709.

HARNED H. S. and DAVIS R. JR (1943) The ionization constant of carbonic acid in water and the solubility of carbon dioxide in water and aqueous salt solutions from 0 to 50°. *Am. Chem. Soc. J.* **65**, 2030–2037.

HELGESON H. C. (1969) Thermodynamics of hydrothermal systems at elevated temperatures and pressures. *Am. J. Sci.* **267**, 729–804.

HOUSE W. A. (1981a) Kinetics of crystallization of calcite from calcium bicarbonate solutions. *J. Chem. Soc. Faraday Trans. I* **77**, 341–359.

HOUSE W. A. (1981b) An experimental investigation of carbon dioxide adsorption during calcite precipitation. *Colloids Surfaces* **2**, 119–131.

JACOBSON R. L. and LANGMUIR D. (1974) Dissociation constants of calcite and $CaHCO_3^+$ from 0 to 50°C. *Geochim. Cosmochim. Acta* **35**, 1023–1045.

JOHNSON N. M. (1979) Acid rain: Neutralization within the Hubbard Brook ecosystem and regional implications. *Science* **204**, 497–499.

KOUTSOUKOS P., AMJAD Z., TOMSON M. B. and NANCOLLAS G. H. (1980) Crystallization of calcium phosphates. A constant composition study. *Am. Chem. Soc. J.* **102**, 1553–1557.

MULLIN J. W. (1972) *Crystallization.* 2d edn. 482 pp. CRC Press.

MULLIN J. W. and OSMAN M. M. (1973) Nickel ammonium sulfate crystal growth rates in aqueous solution. *J. Chem. Eng. Data* **18**, 353–355.

NANCOLLAS G. H. and PURDIE N. (1964) The kinetics of crystal growth. *Quart. Rev. Chem. Soc.* **18**, 1–20.

NANCOLLAS G. H. and REDDY M. M. (1971) The crystallization of calcium carbonate II. Calcite growth mechanism. *J. Colloid Interface Sci.* **36**, 166–172.

NANCOLLAS G. H. and REDDY M. M. (1974a) Crystal growth kinetics of minerals encountered in water treatment processes. In *Aqueous-Environmental Chemistry of Metals* (ed. A. J. Rubin), pp. 219–253. Ann Arbor.

NANCOLLAS G. H. and REDDY M. M. (1974b) The kinetics of crystallization of scale forming minerals. *Soc. Pet. Eng. J.* **14**, 117–126.

NANCOLLAS G. H., AMJAD Z. and KOUTSOUKOS P. (1979) Calcium phosphates—speciation, solubility and kinetic considerations. In *Chemical Modeling in Aqueous Systems.* (ed. E. A. Jenne), pp. 475 497. A.C.S. Symp. Ser. No. 93.

PLUMMER L. N., JONES B. F. and TRUESDELL A. H. (1976) WATEQF-A FORTRAN IV version of WATEQ, a computer program for calculating chemical equilibrium of natural water. *U.S. Geol. Surv. Water-Resour. Invest.*, 76–13, pp. 63.

PLUMMER L. N., WIGLEY T. M. L. and PARKHURST D. L. (1978) The kinetics of calcite dissolution in CO_2-water systems at 5° to 60°C and 0.0 to 1.0 atm CO_2. *Am. J. Sci.* **278**, 179–216.

PLUMMER L. N., WIGLEY T. M. L. and PARKHURST D. L.

(1979) Critical review of the kinetics of calcite dissolution and precipitation. In *Chemical Modeling in Aqueous Systems* (ed. E. A. Jenne), pp. 537–573. A.C.S. Symp. Ser. No. 93.

REARDON E. J. and LANGMUIR D. (1974) Thermodynamic properties of the ion pairs $MgCO_3^0$ and $CaCO_3^0$ from 10 to 50°C. *Am. J. Sci.* **274**, 599–612.

REDDY M. M. (1975) Kinetics of calcium carbonate formation. *Proc. Int. Assoc. of Theoretical and Applied Limnology* **19**, 429–438.

REDDY M. M. (1977) Crystallization of calcium carbonate in the presence of trace concentrations of phosphorus containing anions. I. Inhibition by phosphate and glycerophosphate ions at pH 8.8 and 25°C. *J. Cryst. Growth* **41**, 287–295.

REDDY M. M. (1978) Kinetic inhibition of calcium carbonate formation by wastewater constituents. In *The Chemistry of Wastewater Technology* (ed. A. J. Rubin), pp. 31–58. Ann Arbor.

REDDY M. M. (1979) Distribution, transport, adsorption, and precipitation of inorganic phosphorus in the Genesee River. In *Chemical Modeling in Aqueous Systems* (ed. E. A. Jenne), pp. 737–759. A.C.S. Symp. Ser. No. 93.

REDDY M. M. and NANCOLLAS G. H. (1971) The crystallization of calcium carbonate I. Isotopic exchange and kinetics. *J. Colloid Interface Sci.* **36**, 166–172.

REDDY M. M. and NANCOLLAS G. H. (1973) Calcite crystal growth inhibition by phosphonates. *Desalination* **12**, 61–73.

REDDY M. M. and NANCOLLAS G. H. (1976) The crystallization of calcite carbonate IV. The effect of magnesium, strontium and sulfate ions. *J. Crystal Growth* **35**, 33–38.

TRUESDELL A. H. and JONES B. F. (1974) WATEQ, A computer program for calculating chemical equilibria of natural waters. *U.S. Geol. Survey J. Res.* **2**, 233–248.